

Development of a phenomenological scaling law for fractal aggregate sintering from molecular dynamics simulation

T. Hawa^{a, c}, M.R. Zachariah^{a, b, c, *}

^aDepartment of Mechanical Engineering, University of Maryland, College Park, MD, USA

^bDepartment of Chemistry and Biochemistry, University of Maryland, College Park, MD, USA

^cNational Institute of Standards and Technology, Gaithersburg, MD, USA

Received 8 January 2007; received in revised form 31 May 2007; accepted 31 May 2007

Abstract

A simple modification to the Frenkel sintering law is developed for nanoparticle fractal aggregates, based on molecular dynamics (MD) simulations. The fractal aggregates investigated consist of up to 110 primary particles, with primary particles of 2.5 nm in diameter, and the fractal dimension of 1 (wire), 1.9 (complex), and 3 (compact). In addition simple prototype L- and T-shape aggregate were considered. We found that L-shape aggregates behaved similar to straight chains and thus did not impact the overall sintering time. By contrast T-shape aggregate sintering kinetics was controlled by the longest contiguous branch in the system (i.e. effective primary branch length). We found that sintering of fractal aggregates is a combination of local sintering processes of line-, L- and T-shape structures. As expected, sintering time increases with increasing mass of the aggregate and with decreasing the fractal dimension. The sintering times normalized by the primary particle diameter showed a universal relationship which depends only on the number of particles in an aggregate and its fractal dimension. The MD results were found to be qualitatively consistent with a continuum viscous flow model, and was used as the basis from which a phenomenological sintering law for fractal aggregates could be derived. The phenomenological model is a power law modification of the Frenkel sintering equation to include a dependence on the number of particles in a fractal aggregate and fractal dimension:

$$t = t_{\text{Frenkel}} * (N - 1)^{0.68 \wedge D_f}$$

This relationship is amenable for use in phenomenological aerosol models that might include sintering effects.
Published by Elsevier Ltd.

Keywords: Sintering; Scaling laws; Aggregates; Molecular dynamics

1. Introduction

Nanoparticles and nanocrystals, whose sizes range from 1 to 100 nm are often assembled as large aggregates or agglomerates (Barnes, Mahurin, Mehta, Sumpter, & Noid, 2002; Helble & Sarofim, 1989). At this length scale, the particle melting point decreases, optical and chemical properties change relative to bulk materials (Alivisatos, 1996; Colvin, Alivisatos, & Tobin, 1991; Goldstein, Echer, & Alivisatos, 1992; Shi, Gider, Babcock, & Awschalom, 1996; Xing & Rosner, 1999). The specific surface area or its related primary particle diameter are mostly used to characterize

* Corresponding author. Department of Chemistry and Biochemistry, University of Maryland, College Park, MD, USA.
E-mail address: mrz@umd.edu (M.R. Zachariah).

commercially produced nanoparticles. However, applications of nanoparticles require specific properties that also depend strongly on structure, particularly as they relate to structural composites. Thus, control of particle morphology is critically important to create or preserve a desired material property.

Gas phase production is generally the method of choice by industries that requires large scale production, or ultraclean materials (Frenkel, 1945; Kruis, Fissan, & Peled, 1998). However, high volume fraction gas phase synthesis typically results in highly aggregated structures. Depending on the desired end use of the particles, different primary particle sizes and extents of agglomeration are desired. In many cases the main focus is towards minimizing agglomeration (Xiong, Akhtar, & Pratsinis, 1993), while for example in application to energetic materials, the main focus is to minimize the primary particle size so as to increase the exposed surface area of an aggregate cluster available for reaction (Park, Lee, Rai, Mukherjee, & Zachariah, 2005). The collision–sintering mechanism of particle growth is considered to control primary particle diameter and aggregate shape in the gas-phase production process (Friedlander, 2000). The particle growth mechanisms nominally includes nucleation, condensation, coagulation and sintering. The competition between the rates of coagulation and sintering serve to define the freezing-in of the primary particle size and the onset of aggregate formation (Friedlander, 2000; Lehtinen & Zachariah, 2001, 2002; Mukherjee, Sonwane, & Zachariah, 2003). Therefore, particle morphology and size can be controlled by either modifying the characteristic sintering or collision time. To define a characteristic sintering time for an aggregate a greater extent of understanding than is currently available is required.

In an effort to understand the particle growth mechanism described above, a variety of numerical and analytical studies were conducted. For two bare particles of equivalent size, the characteristic sintering time is obtained from either phenomenological solid state diffusion (Friedlander & Wu, 1994) or viscous flow (Frenkel, 1945) models (e.g. SiO₂ is known as to grow by a viscous diffusion process). In prior studies we investigated using molecular dynamics (MD) simulation, the characteristic coalescence times for binary particles, and compared them with phenomenological models (Zachariah & Carrier, 1999). Recently we also investigated surface (hydrogen) passivation on the sintering and morphology of silicon nanoparticle, and presented a phenomenological model to describe the dynamics during the sintering of these coated particles (Hawa & Zachariah, 2005). Our model, extended from the Frenkel model, was able to describe the entire sintering process. More recently, we focused on understanding the sintering mechanisms of unequal sized, and bare nanoparticles (Hawa & Zachariah, 2006). We found that the Koch–Friedlander model accurately predicted the sintering time of two unequal sized particles for both bare and coated cases, when benchmarked against the MD simulation results. We also found that the characteristic sintering times are independent of the volume ratio of the coalescing partners. Yadha and Helble also investigated the sintering of unequally sized particle coalescence prior to our study using the analytical expression for the surface geometry to achieve computation efficiency (Yadha & Helble, 2004).

However, all these studies focus on the kinetics of binary pairs of particles.

Several researchers have approached the problem of aggregate sintering using Monte-Carlo or other Brownian dynamics approaches. Prior work includes a Monte-Carlo grid-base approach for 2D sintering model assuming particles take random walks on the surface of the aggregate (Akhtar, Lipscomb, & Pratsinis, 1994). Recently, Kulkarni and Biswas (2003) introduced a simple Brownian dynamics simulation approach to understand the evolution of morphology of a sintering deposit. Their sintering model conserves mass, and computes the associated surface area based on a sintering model proposed by Friedlander and Wu (1994). However, during sintering their particles retain a single point contact without merging with each other, and assume a radius shrinkage for one particle and growth for the other as a means to conserve mass. Schmid, Tejwani, Artelt, and Peukert (2004) considered that the sintering particles are merging, and the remaining parts of the two particles maintain a spherical shape, much like Frenkel's model.

In all the approaches above, simulation of aggregate sintering required an *a priori* assumption as to how sintering would occur in an aggregate, and then applying a standard sintering approach to map the evolution of the morphology.

Recently, we investigated how aggregate sintering might occur without resorting to a preconceived model, using atomistic simulation to probe how it might differ from the simplest case of binary particles (Hawa & Zachariah, 2007). The chain aggregates investigated consisted of up to 80 primary particles of silicon, with primary particles of 2.5–7 nm in diameter. We found that sintering of chain aggregates consists of three steps: (a) reaction between particles to minimize surface defects and development of a cylindrical like shape, comprised an induction period. A second step (b) consisted of contraction of the cylinder, which actually consisted of two contraction stages. The first stage was the local contraction stage where sintering occurs only at the ends of the particle chain, and the second stage involves the global contraction. The last step was the nominal sintering process from an oval to spherical shape. As expected, sintering time

increases with increasing chain length, with the exception that very long chains fragmented. Interestingly, the sintering times normalized by the primary particle diameter showed a universal relationship which only depends on chain length. These results were found to be consistent with a mathematical model we developed, based on continuum viscous flow. The model assumes that steps (b)–(c) dominate the entire sintering process of chain aggregates, and neglects the initial and final processes from our mathematical model for simplicity. The justification for this assumption comes from our MD simulation that shows that the formation of the cylinder from the aggregate chain is very rapid. From continuity, we obtain

$$\frac{dL}{dt} = -\alpha \frac{L}{2}, \quad (1)$$

where L is the chain length, $\alpha/2$ is the linear compression coefficient per unit time and t is time. From a balance between the surface energy, and energy dissipation due to viscosity, we obtain

$$-\sigma\pi r \left[1 + \frac{1}{2} \left(\frac{r}{L} \right) \right] \frac{dL}{dt} = 3\eta\alpha^2\pi r^2 L, \quad (2)$$

where σ denotes the surface tension, η denotes the viscosity and r denotes the radius of the cylinder. Substituting the expression (1) into (2) and integrating over the process of the contraction of cylinder from the initial chain length, L_0 , to $(4V/\pi)^{1/3}$, i.e. when the diameter of the cylinder is equal to the length of the cylinder, where V is the total volume of the column, gives the time required for the sintering of the chain aggregates as

$$t = \frac{\eta}{\sigma} \left(\frac{2V}{\pi} \right)^{1/3} (A + B + C), \quad (3)$$

where

$$A = -2\sqrt{3} \left\{ A \tan \left[\frac{1 - 2^{5/3}}{\sqrt{3}} \right] - A \tan \left[\frac{1 - 2(2\sqrt{\pi/V})^{1/3}\sqrt{L_0}}{\sqrt{3}} \right] \right\},$$

$$B = -2 \left\{ \ln \left[1 + 2^{2/3} \right] - \ln \left[1 + \left(2\sqrt{\frac{\pi}{V}} \right)^{1/3} \sqrt{L_0} \right] \right\} \quad \text{and}$$

$$C = \ln \left[1 - 2^{2/3} + 2^{4/3} \right] - \ln \left[1 - \left(2\sqrt{\frac{\pi}{V}} \right)^{1/3} \sqrt{L_0} + \left(2\sqrt{\frac{\pi}{V}} \right)^{2/3} L_0 \right],$$

where σ denotes the surface tension of the material, η is the viscosity, L_0 is the initial chain length and V is the total volume of the aggregate.

This model was able to predict the sintering time in excellent agreement with results obtained from MD simulation for any chain length, and any primary particle size for straight nanoparticle chain aggregates. The results for sintering times for aggregate chains could be summarized with a power law modification of the Frenkel viscous flow equation, to include a dependence on the number of particle connections ($N - 1$) in a chain aggregate:

$$t = t_{\text{Frenkel}} * (N - 1)^{0.68}, \quad (4)$$

where $t_{\text{Frenkel}} = 4\eta a_0/3\sigma$, and a_0 is the initial radius of the particle (Hawa & Zachariah, 2007). Although both the above scaling law, and the viscous flow model for straight aggregate chains (which can also be applied for sintering of nanowires) agree with the MD simulations results, gas phase synthesis generally produces highly complex aggregated structures, especially if coagulation and sintering occur simultaneously and at a similar rate. Monte-Carlo simulations have shown a strong dependence of the fractal dimension on the sintering process (Schmid et al., 2004). MD simulations of sintering of aggregate nanoparticles will provide a more detailed dynamics of the sintering mechanism, and ideally lead to a simple scaling law for sintering of fractal aggregates.

In this paper we focus on sintering of various geometric representations of aggregates, from simple to complex structures. We consider a single secondary branch from the primary branch, like L- and T-shape structure, and the aggregate structures of fractal dimension of 1.9 (typical aggregates seen in gas-phase process) and 3 (compact structure).

The primary particle sizes are equal in this study. We will use MD simulation to track the evolution of a sintering process and compute the sintering time. We will investigate the applicability or modification to the two-particles sintering model (Frenkel, 1945) for complex aggregates, and will present a scaling law of nanoparticle aggregates as a function of fractal dimension. We clarify the relationship between aggregate mass and the fractal dimension in the dynamics of sintering, and provide insight into the relationship between the model of scaling law, and the MD simulation results, and identify the mechanism of sintering for complex aggregates.

2. Computational model and numerical procedure

To track sintering process we employ an atomistic simulation approach using classical MD. For this study we use the SW potential for silicon (Stillinger & Weber, 1985). While similar sets of potential energy functions have also been developed by Tersoff (1986, 1988a,b, 1989), the SW potential is designed to describe interactions in both solid and liquid forms of silicon. Since most synthesis processes leading to cluster formation occur at high temperature, cluster growth by sintering is dominated by liquid-like characteristics, and the accuracy of the SW potential increases with increasing particle size or temperature. The SW potential energy, V , is a sum of two and three-body interactions given by

$$V = \sum_{\substack{i,j \\ i < j}} V_2(i, j) + \sum_{\substack{i,j,k \\ i < j < k}} V_3(i, j, k), \quad (5)$$

where the two-body term is

$$V_2(r_{ij}) = \begin{cases} \alpha_{ij}(\beta_{ij}r_{ij}^{-p} - 1) \exp[a_{ij}/(r_{ij} - b_{ij})], & r_{ij} < b_{ij}, \\ 0, & r_{ij} \geq b_{ij} \end{cases}$$

and the three-body term is

$$V_3(r_{ij}, r_{jk}, r_{ki}) = h(r_{ij}, r_{ik}, \theta_{jik}) + h(r_{jk}, r_{ji}, \theta_{ijk}) + h(r_{ki}, r_{kj}, \theta_{jki}),$$

where h is

$$h(r_{ij}, r_{ik}, \theta_{jik}) = \begin{cases} \lambda_{jik}(1 + \mu_{jik} \cos \theta_{jik} + \nu_{jik} \cos^2 \theta_{jik}) \exp \left[\frac{\gamma_{ij(k)}}{r_{ij} - \chi_{jik}} + \frac{\gamma_{ik(j)}}{r_{ik} - \chi_{jik}} \right] & \text{if } r_{ij} < \chi_{jik} \text{ and } r_{ik} < \chi_{jik}, \\ 0 & \text{otherwise.} \end{cases}$$

r is the distance between a pair of atoms, b_{ij} and χ_{jik} are the cutoff distance of the two-body and the three-body potentials and θ_{ijk} is the vertex angle at j subtended by i and k . α_{ij} , β_{ij} , p , a_{ij} , and λ_{jik} , μ_{jik} , ν_{jik} , $\gamma_{ij(k)}$, and $\gamma_{ik(j)}$ are fixed parameters chosen for liquid silicon (Stillinger & Weber, 1985).

All simulations were run on the JVN Linux Cluster running up to 32 processors. Atom trajectories were determined by integrating the classical equations of motion using the velocity form of the Verlet algorithm (Verlet, 1967), with rescaling of atomic velocities at each time step to achieve temperature control. Time steps of 0.5 fs were typically used to ensure energy conservation, and a Verlet neighbor list with parallel architecture was employed in all the simulations, with a neighbor list renewal every 10 steps. The simulations take place in a spherical cavity of 200 nm radius using an elastic boundary condition.

The first step in the equilibration process was to prepare silicon particles of 500 Si atoms at 2100 K. After removal of angular momentum, particle temperatures were reduced slowly to 1500 K and equilibrated for 50 ps. For the last step in the preparation process, the simulations were switched to a constant energy calculation for 20 ps. If the average temperature of the particle deviated by more than 10 K over this period, the equilibration process was repeated until the particle temperature deviated by less than 10 K.

Duplicated particles were generated, placed on a geometry given for the appropriate aggregates initially in contact with each other. We study the aggregate structure of L- and T-like shape, and fractal dimensions of 1 (wire structure), 1.9 (typical aggregate seen in gas-phase synthesis), and 3 (compact structure). Sintering is exothermic, therefore there is the potential that the temperature would increase, and affect properties such as diffusivity, which would significantly

alter the kinetics (Lehtinen & Zachariah, 2001; Zachariah & Carrier, 1999). In order to simplify this problem we chose to study the sintering process under constant temperature conditions at 1500 K. In point of fact for a real growth process, particles of this size would not see temperature excursions, since they are effectively thermostated by the surrounding gas (Mukherjee et al., 2003).

3. Results and discussion

3.1. L-shape aggregate

We begin with a simulation of a simple aggregate, which has a straight secondary branch at a right angle from the end of a straight primary branch. Fig. 1 presents the temporal evolution for the L-shape aggregate composed of 40 primary particles of 500 Si atoms each (Fig. 1(a)). The primary and secondary branches contain 34 and 6 primary particles, respectively. The L-shape aggregate initially develops a smooth surface curvature, and the right angle corner quickly

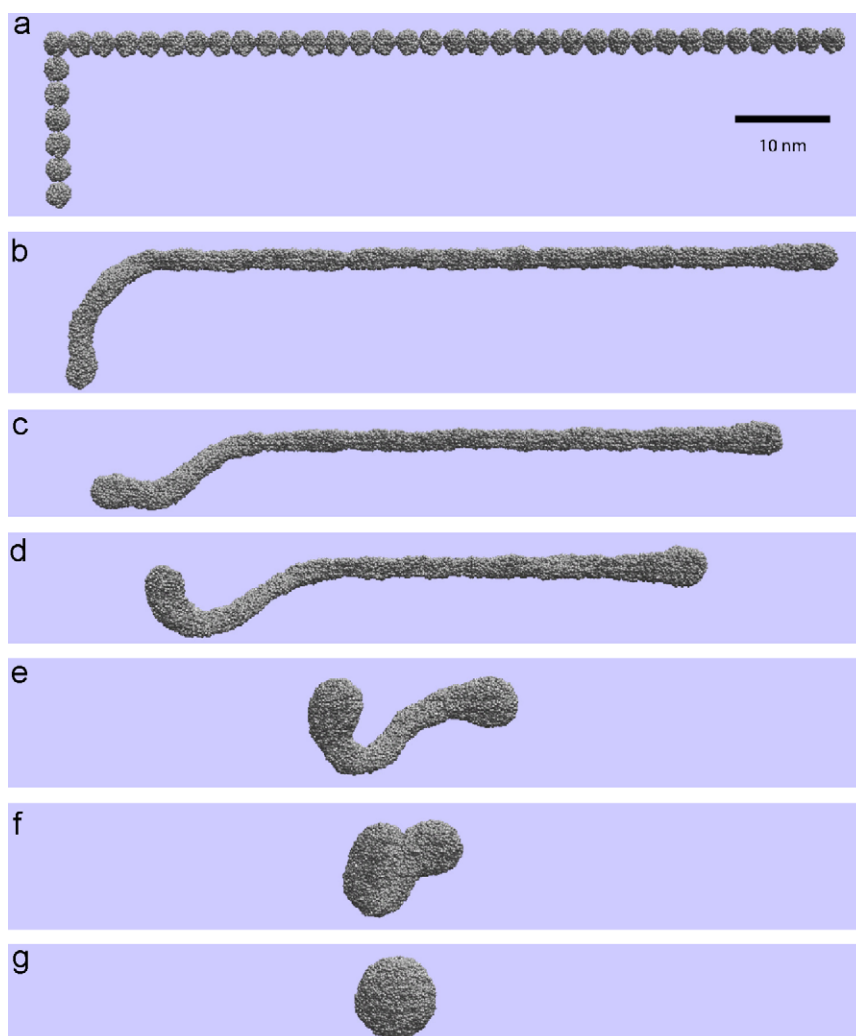


Fig. 1. Temporal snapshots of the morphology during sintering of a 40 particle L-shaped chain aggregate with 500 atoms in a particle at 1500 K. Primary and secondary branches contain 34 and 6 particles. (a) $t = 0$ ps, (b) $t = 13$ ps, (c) $t = 29$ ps, (d) $t = 47$ ps, (e) $t = 86$ ps, (f) $t = 97$ ps and (g) $t = 130$ ps.

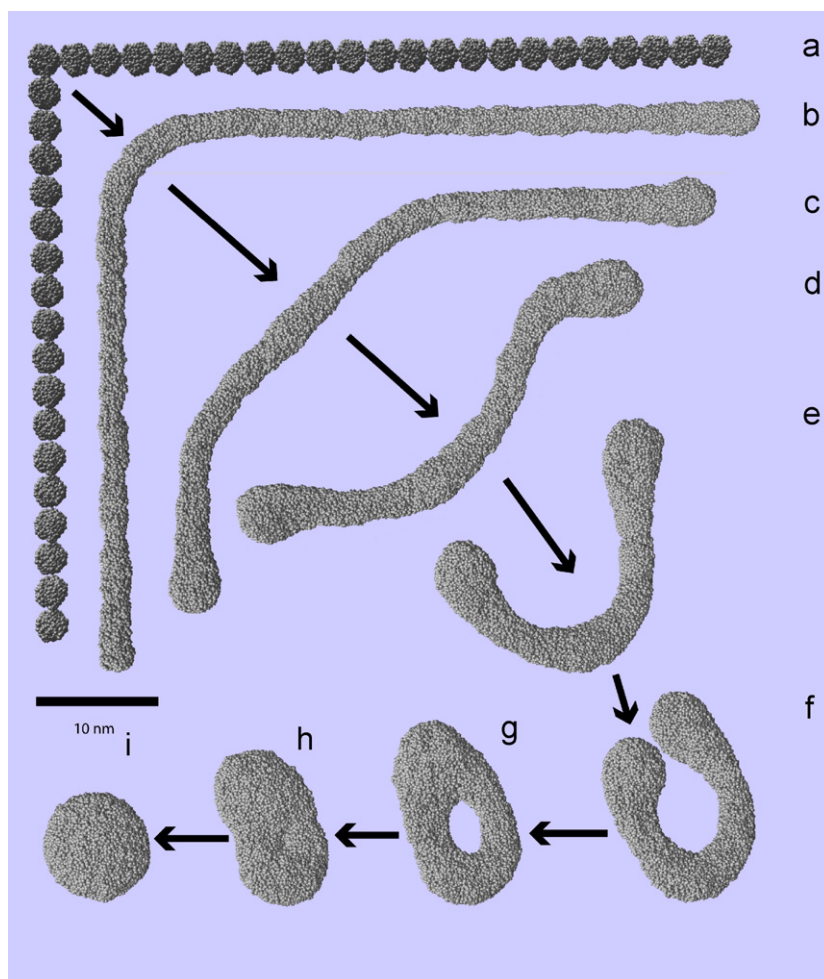


Fig. 2. Temporal snapshots of the morphology during sintering of a 40 particle L-shaped chain aggregate with 500 atoms in a particle at 1500 K. Primary and secondary branches contain 23 and 17 particles. (a) $t = 0$ ps, (b) $t = 14$ ps, (c) $t = 37$ ps, (d) $t = 62$ ps, (e) $t = 79$ ps, (f) $t = 90$ ps, (g) $t = 95$ ps, (h) $t = 105$ ps and (i) $t = 133$ ps.

forms a rounded shape (Fig. 1(b)). A portion of the secondary branch smoothly merged with the primary branch. Then, the primary branch, column like shape, shrinks to minimize its surface area, and mass accumulates at the ends of the rod (Fig. 1(c)). This is similar to what we have found in the previous study of sintering of straight chain aggregate and formation of a dumbbell-like structure (Hawa & Zachariah, 2007). Basically what is happening is that atoms in the center of the cylinder are being pulled by neighbors on either axial side, while atoms at the end of the aggregate have neighbors only to one side, so that as the aggregate tries to coalesce, it is easier for the end of the rod to grow. As the right angle begins to straighten, angular momentum forces create a whip-like motion to the end (Fig. 1(d)), which eventually results in the end of the chain meeting the body of the chain (Fig. 1(f)).

We also consider the case that the length of the primary branch is comparable to that of the secondary branch. Fig. 2(a) shows an L-shape aggregate whose primary and secondary branch contain 23 and 17 primary particles. The initial behavior is similar to the short branch case (Fig. 2(b)). However the angular momentum induced whip-like action is considerably more pronounced and results in the ends of the chain curving together to form a toroidal structure (Fig. 2(f,g)). In contrast to the short branch case which behaved like a small perturbation to the straight chain case, a larger secondary branch changes the dynamics of the overall sintering dramatically.

The sintering time as a function of the ratios of secondary to primary branch length are summarized in Fig. 3, for an aggregate of 40 primaries of 500 atoms each. The normalized sintering time is defined relative to the corresponding

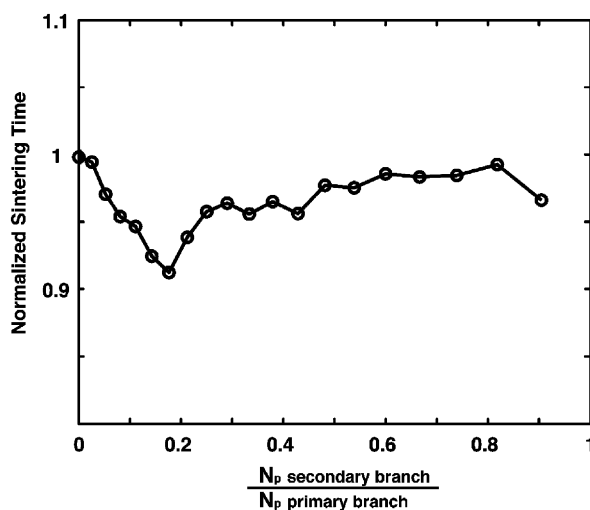


Fig. 3. Sintering time of L-shaped aggregates normalized by the straight chain aggregate containing the same number of particles as a function of the ratio of secondary to primary branch length. The sintering time of the straight chain aggregate is 139 ps.

straight chain aggregate containing the same number of total primary particles, whose sintering time is 138 ps. Even though the dynamics of sintering process are dramatically different from small to large branch ratios as seen from Figs. 1 and 2, it does not affect to total sintering time, whose deviation is within $\pm 4.5\%$. This result indicates that the L-shape aggregate, behaves much like a straight chain, and thus, the effective primary branch is the total length of the L-shape aggregate. As long as the bending angle is not acute, so as to fold both branches during their sintering process, sintering is equivalent to shrinking of a single branch, and the energy consumed during the flipping motion is negligible.

3.2. T shape aggregates

We also study a simple aggregate, which has a straight secondary branch protruding perpendicularly from the center of the straight primary branch. Fig. 4 presents the temporal evolution for the T-shape aggregate composed of 40 primary particles of 500 Si atoms (Fig. 4(a)). In the example illustrated the primary and secondary (middle) branches contain 35 and 5 primary particles. The T-shape aggregate initially develops a smooth surface curvature, and the intersection of both branches evolves rapidly to a larger primary particle (Fig. 4(c)). In this case the memory of the branch is retained as an obvious large primary particle in the center of the structure for essentially the entire sintering event.

We also consider the case that the length of the primary branch is comparable to that of the secondary branch. Fig. 5(a) shows a T-shape aggregate whose primary and middle branch contain 21 and 19 primary particles. Because of the size of the middle branch it cannot sinter as rapidly as the previous example to form a large primary (Fig. 5(b)). Rather, since the original length of top and bottom portion of primary branch is half that of the middle branch, both ends of primary branch move toward each other due to the movement of the intersection toward the middle branch to form a “Y” structure (Fig. 5(c)). Subsequently this “Y” closes on itself to form a straight chain with a drumstick like structure (Fig. 5(d)). Unlike the previous case, the middle portion of the aggregate is now the thinnest part of the aggregate, similar to the straight chain aggregate.

Sintering time as a function of ratios of number of particles in a middle branch to the entire aggregate is summarized in Fig. 6. The vertical axis is the sintering time normalized by the straight chain aggregate containing the same number of total primary particles (40). When the middle branch is short, sintering of the T-shape aggregate approximated as that of straight chain aggregate with a small disturbance at the center. Thus, the sintering time is determined by the initial length of the primary branch. The minimum sintering time is about the 70% of the straight chain aggregate containing the same number of total primary particles and found at the ratio of 0.28, which is slightly smaller than a value of 0.33 which corresponds to the middle branch, top and bottom portion of the primary branches of equal length. Above the critical ratio of 0.28, the sintering time monotonically increases with the ratio.

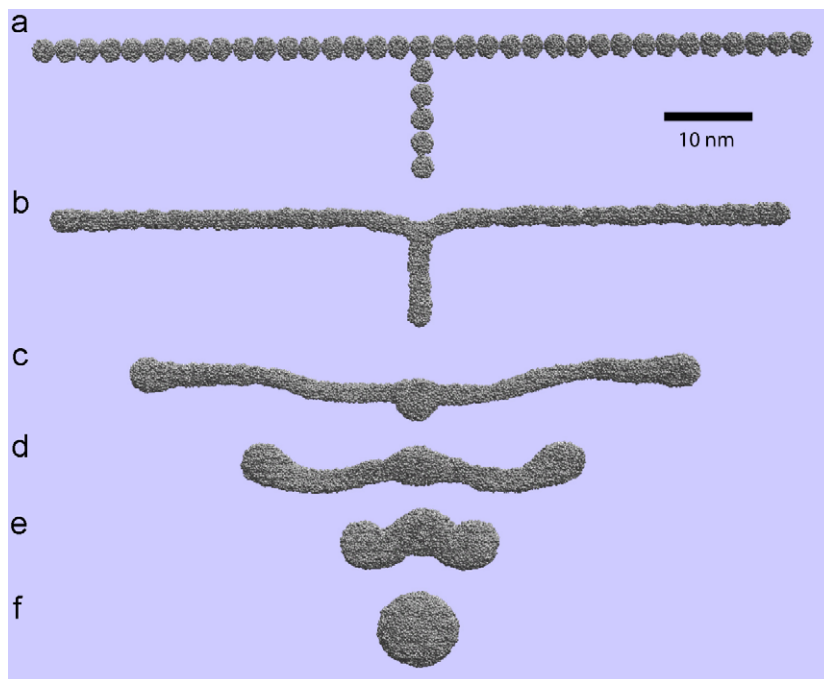


Fig. 4. Temporal snapshots of the morphology during sintering of a 40 particle T-shaped chain aggregate with 500 atoms in a particle at 1500 K. Primary and middle branches contain 35 and 5 particles. (a) $t = 0$ ps, (b) $t = 13$ ps, (c) $t = 36$ ps, (d) $t = 58$ ps, (e) $t = 87$ ps and (f) $t = 122$ ps.

Both L- and T-shape aggregate studies indicate that the primary branch length determines the sintering time. What determines the definition of the primary branch, is the longest contiguous chain length. In some cases for the T-shaped aggregate this might be the vertical of the T and half the horizontal, if the vertical is longer than the horizontal.

We plot the sintering time of the T-shape aggregate normalized by primary particle diameter as a function of number of particles in an effective primary branch in Fig. 7. The choice of plotting the MD results in terms of a sintering time normalized by the primary particle diameter is based on our phenomenological model sintering time, developed in the previous study of straight chain aggregates, which shows a linear dependence on diameter (see Eq. (3)) (Hawa & Zachariah, 2007). The solid line represents the sintering time for straight chain aggregates (fractal dimension, $D_f = 1$) obtained from a scaling law modification of the Frenkel viscous flow equation, to include a dependence on the number of particle connections in a chain aggregate (Eq. (4)). MD simulation results show excellent agreement with the power law model. This indicates that the effective primary branch length dominates the sintering process of the simple chain aggregates, and that secondary branches are small disturbance to the primary branch.

3.3. Aggregates of fractal dimension 1.9

Even though the above simple structure of chain aggregates agree with the power law model for the effective primary branch analysis, gas phase synthesis generally produces highly complex aggregated structures. We turn our attention to address how to employ the analysis developed to this point for computing the sintering of fractal structures.

Aggregates grown in the aerosol phase typically form from cluster–cluster aggregation events which lead to aggregates of fractal dimension < 2 . Aggregates of $D_f = 1.9$ consisting of 17, 32, 52, 66 and 110 primary particles were prepared from the coordinates produced via Brownian dynamics (Mulholland, Bohren, & Fuller, 1994). Fig. 8 presents the structure and temporal evolution for a 66 primary particle aggregate. The fractal aggregate initially develops a smooth surface curvature, and the initially complicated structure forms multiple secondary branches. The longest contiguous length to define the primary branch is shown as the dotted line in Fig. 8(b). Each of the secondary branches connected to the primary branch can now be viewed in the context of a “T” or “L” shaped aggregate. Sintering of the short secondary branches occurs in manner similar to that observed for the prototype “T” and “L” shaped aggregates discussed in the

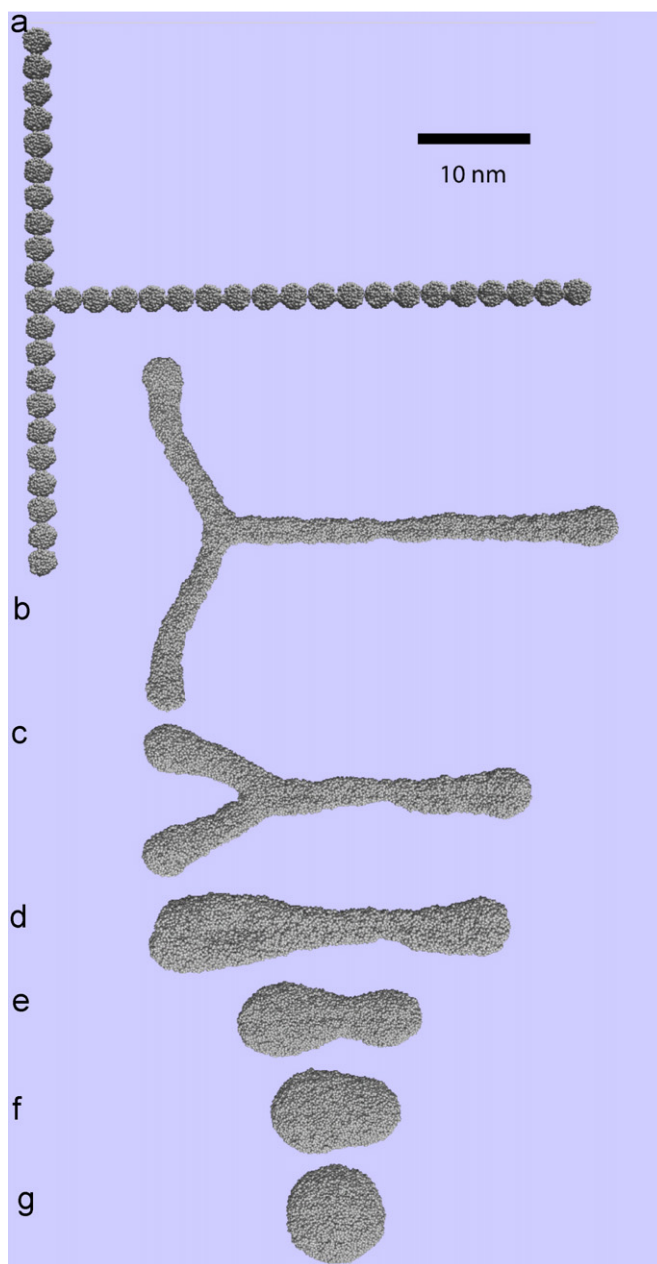


Fig. 5. Temporal snapshots of the morphology during sintering of a 40 particle T-shaped chain aggregate with 500 atoms in a particle at 1500 K. Primary and middle branches contain 21 and 19 particles. (a) $t = 0$ ps, (b) $t = 25$ ps, (c) $t = 50$ ps, (d) $t = 62$ ps, (e) $t = 75$ ps, (f) $t = 94$ ps and (g) $t = 116$ ps.

previous sections (Fig. 8(c,d)). However, one significant difference is that there is no large scale motion of the structure as was seen in Figs. 2 and 5 since the branches are well distributed in all directions. Essentially then any fractal aggregate can be thought of as an assembly of “T” and “L” aggregates.

We had previously shown in our analysis of straight chain aggregates that the sintering time normalized to the primary particle size gives a universal sintering relationship that only depends on chain length for straight chain aggregates (Hawa & Zachariah, 2007) (i.e. $D_f = 1$) as shown in Fig. 9. Moreover, the viscous flow model showed excellent

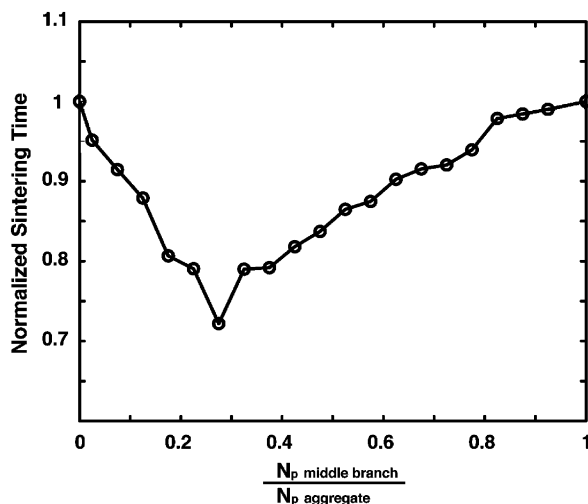


Fig. 6. Sintering time of T-shaped aggregates normalized by the straight chain aggregate containing the same number of particles as a function of ratios of number of particles in a middle branch to an entire aggregate. The sintering time of the straight chain aggregate is 139 ps.

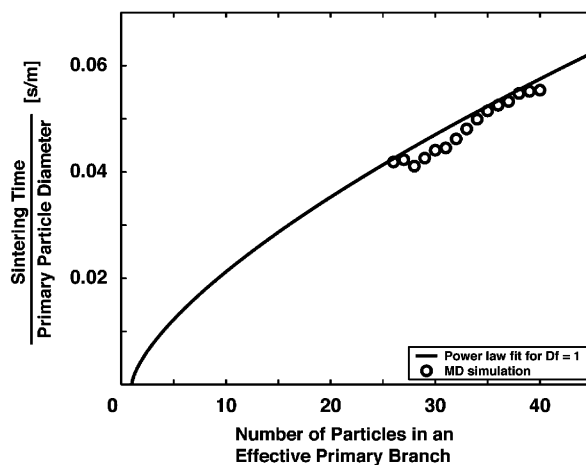


Fig. 7. A comparison of MD sintering time of T-shaped aggregates normalized by primary particle diameter with scaling law model for a chain aggregate. Horizontal axis is the number of particles in an effective primary branch.

agreement for all lengths and sizes of chain aggregates, and we approximated the sintering time for straight chain aggregates as a function of chain length (Eq. (4)).

We can now extend this analysis to a structure of arbitrary fractal dimension. In a similar way we plot the MD simulated sintering time of the fractal aggregate of $D_f = 1$, 1.9 and 3 normalized by primary particle diameter, vs. number of particles in the aggregate (or mass of the aggregate) in Fig. 10. The definition of $D_f = 3$ in this study is that all primaries are placed to form a compact and symmetry aggregate with respect to the principal axes of the structure. As with other kinds of fractal aggregates, primaries are initially in contact each other. By plotting the normalized sintering time we obtain results that are independent of primary particle diameter, and only depends on the number of primary units. The results for these three very different fractal dimensions are a monotonic increase in sintering time with the total number of particles in the aggregate.

When $D_f = 1$ and 3, the data points correspond to the MD simulations and indicate a monotonic increase in sintering time with increasing number of particles in the aggregates. A comparison with the scaling law model for these three cases is shown as a solid line in the figure. We approximate the sintering time for a fractal aggregate as a modification

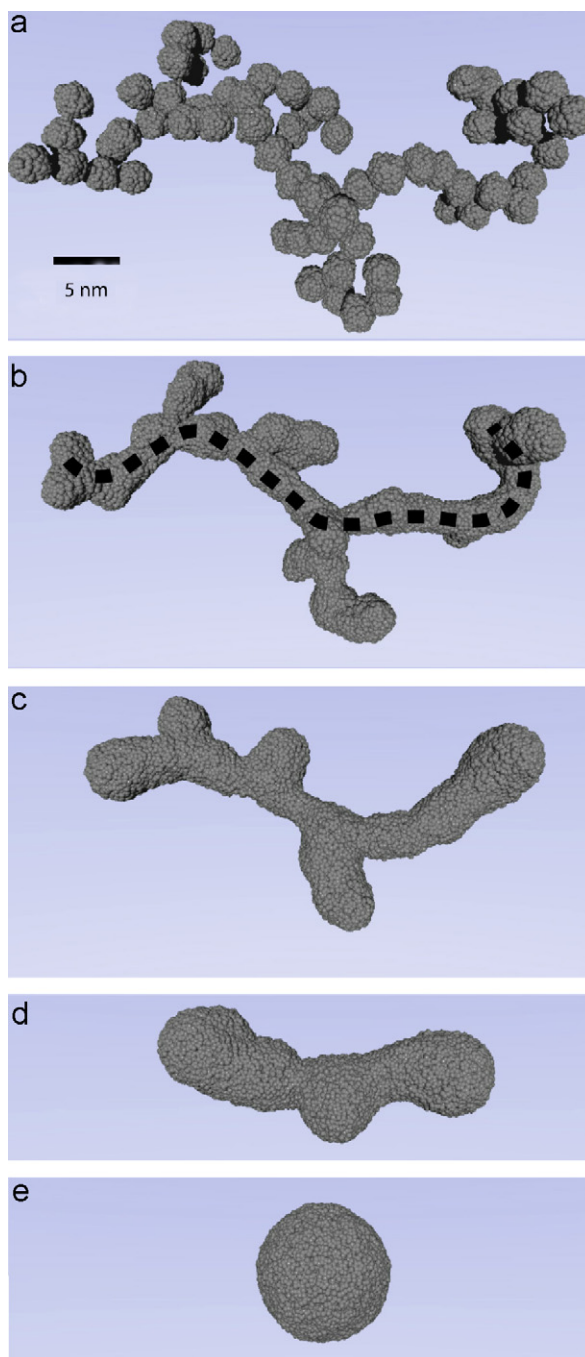


Fig. 8. Temporal snapshots of the morphology during sintering of a 66 particle aggregate with its fractal dimension 1.9 at 1500 K. (a) $t = 0$ ps, (b) $t = 23$ ps, (c) $t = 41$ ps, (d) $t = 69$ ps and (e) $t = 109$ ps.

of the Frenkel model by

$$t = t_{\text{Frenkel}}(N - 1)^{m^{D_f}}, \quad (6)$$

where N is the number of the particles in an aggregate and m is a power constant fit to the results presented and yields a result of $m = 0.68$ as obtained in the previous study for straight chains (Hawa & Zachariah, 2007). $t_{\text{Frenkel}} = 4\eta a_0/3\sigma$,

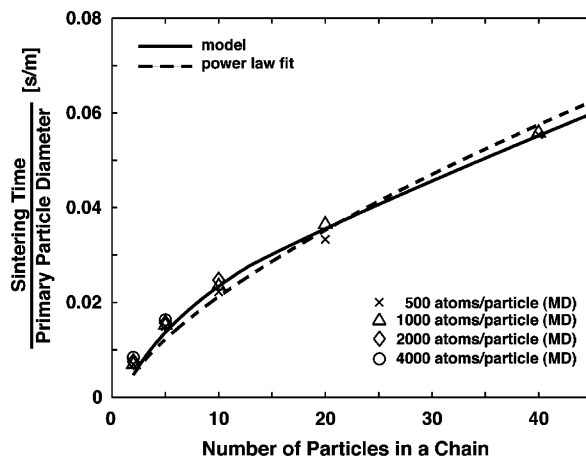


Fig. 9. Sintering times per primary particle diameter vs. as number of particles in a chain, for 500, 1000, 2000 and 4000 atoms/particle. Symbols, MD results; solid line, model; dashed line, power law curve fit.

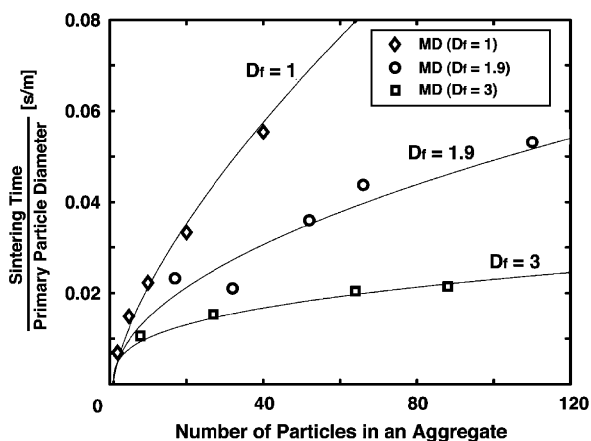


Fig. 10. A comparison of MD sintering time of fractal aggregates at fractal dimension of 1, 1.9 and 3 normalized by primary particle diameter with scaling law model for an aggregate. Horizontal axis is the number of particles in an aggregate.

where $\eta = 5.9$ centipose, $\sigma = 0.826 \text{ J/m}^2$, and $a_0 = 1.25 \text{ nm}$, is the initial radius of the particle (Hawa & Zachariah, 2007). Our model shows excellent agreement for all sizes and fractal dimensions of aggregate nanoparticles. The comparison indicates that this fit provides an extremely convenient way to incorporate aggregate sintering into an aerosol model, since the number of particles, N , can be estimated from the mass of the aggregate and the primary particle size.

4. Conclusion

We extend our prior MD simulations (Hawa & Zachariah, 2007) on straight chain aggregates to investigate the sintering of fractal aggregates. We considered the particle aggregates containing up to 110 and primary particles of 2.5 (500 atoms/particle) in diameter. We studied sintering of simple prototype L- and T-shape aggregates as well as wires, fractal dimension = 1 and compact aggregates of fractal dimension = 3. Finally we turned to fractals that are typical of vapor grown materials with a fractal dimension of 1.9. We found that sintering of fractal aggregates consists of three steps, (a) reaction between particles to minimize surface defects; (b) sintering of multiple secondary branches to the primary branch, and contraction of the primary branch; and (c) the last step was the nominal sintering process

from an oval to spherical shape. We found that L-shape aggregates behaved similar to straight chains and thus did not impact the overall sintering time. By contrast, T-shape aggregate sintering kinetics was controlled by the longest contiguous branch in the system (i.e. effective primary branch length). We found that sintering of fractal aggregates is a combination of local sintering processes of line-, L- and T-shape structures. As expected, sintering time increases with increasing mass of the aggregates and with decreasing fractal dimension. The sintering times normalized by the primary particle diameter showed a universal relationship which depends on the number of particles in an aggregate and its fractal dimension. The results for sintering times for aggregate chains could be summarized with a power law modification of the Frenkel viscous flow equation, which depends on the number of particles in a fractal aggregate and its fractal dimension. $t = t_{\text{Frenkel}} * (N - 1)^{0.68 \wedge D_f}$.

This scaling law model was able to predict the sintering time with excellent agreement to the results obtained from MD, for any size and fractal dimension of aggregate.

Acknowledgments

Support for this work comes from the National Science Foundation and the National Institute of Standards and Technology.

References

- Akhtar, M. K., Lipscomb, G. G., & Pratsinis, S. E. (1994). Monte Carlo simulation of particle coagulation and sintering. *Aerosol Science and Technology*, 21, 83.
- Alivisatos, A. P. (1996). Semiconductor clusters, nanocrystals, and quantum dots. *Science*, 271, 933.
- Barnes, M. D., Mahurin, S. M., Mehta, A., Sumpter, B. G., & Noid, D. W. (2002). Three-dimensional photonic “molecules” from sequentially attached polymer-blend microparticles. *Physical Review Letters*, 88, 015508.
- Colvin, V. L., Alivisatos, A. P., & Tobin, J. G. (1991). Valence-band photoemission from a quantum-dot system. *Physical Review Letters*, 66, 2786.
- Frenkel, J. (1945). Viscous flow of crystalline bodies under the action of surface tension. *Journal of Physics*, 9, 385.
- Friedlander, S. K. (2000). Smoke, dust, and haze: Fundamentals of aerosol dynamics. *Topics in chemical engineering*. USA: Oxford University Press.
- Friedlander, S. K., & Wu, M. K. (1994). Linear rate law for the decay of the excess surface area of a coalescing solid particle. *Physical Review B*, 49, 3622.
- Goldstein, A. N., Echer, C. M., & Alivisatos, A. P. (1992). Melting in semiconductor nanocrystals. *Science*, 256, 1425.
- Hawa, T., & Zachariah, M. R. (2005). Coalescence kinetics of bare and hydrogen-coated silicon nanoparticles: A molecular dynamics study. *Physical Review B*, 71, 165434.
- Hawa, T., & Zachariah, M. R. (2006). Coalescence kinetics of unequal sized nanoparticles. *Journal of Aerosol Science*, 37, 1.
- Hawa, T., & Zachariah, M. R. (2007). Molecular dynamics simulation and continuum modeling of straight chain aggregate sintering: Development of a phenomenological scaling law. *Physical Review B*, in press.
- Helble, J. H., & Sarofim, A. F. (1989). Factors determining the primary particle size of flame-generated inorganic aerosols. *Journal of Colloid and Interface Science*, 128, 348.
- Kruis, F. E., Fissan, H., & Peled, A. (1998). Synthesis of nanoparticles in the gas phase for electronic, optical and magnetic applications—a review. *Journal of Aerosol Science*, 29, 511.
- Kulkarni, P., & Biswas, P. (2003). Morphology of nanostructured films for environmental applications: Simulation of simultaneous sintering and growth. *Journal of Nanoparticle Research*, 5, 259.
- Lehtinen, K. E., & Zachariah, M. R. (2001). Effect of coalescence energy release on the temporal shape evolution of nanoparticles. *Physical Review B*, 63, 205402.
- Lehtinen, K. E., & Zachariah, M. R. (2002). Energy accumulation during coalescence and coagulation of nanoparticles. *Journal of Aerosol Science*, 33(2), 357–368.
- Mukherjee, D., Sonwane, C. G., & Zachariah, M. R. (2003). Kinetic Monte-Carlo simulation of the effect of coalescence energy release on the size and shape evolution of nanoparticles grown as an aerosol. *Journal of Chemical Physics*, 119, 3391.
- Mulholland, G. W., Bohren, C. F., & Fuller, K. A. (1994). Light scattering by agglomerates: Coupled electric and magnetic dipole method. *Langmuir*, 10, 2533.
- Park, K., Lee, D., Rai, A., Mukherjee, D., & Zachariah, M. R. (2005). Size resolved kinetics measurements of aluminum nanoparticle oxidation by single particle mass spectrometry. *Journal of Physical Chemistry B*, 109, 7290.
- Schmid, H. J., Tejwani, S., Artelt, C., & Peukert, W. (2004). Monte Carlo simulation of aggregate morphology for simultaneous coagulation and sintering. *Journal of Nanoparticle Research*, 6, 613.
- Shi, J., Gider, S., Babcock, K., & Awschalom, D. D. (1996). Magnetic clusters in molecular beams, metals, and semiconductors. *Science*, 271, 937.
- Stillinger, F. H., & Weber, T. A. (1985). Computer simulation of local order in condensed phase of silicon. *Physical Review B*, 31, 5262.
- Tersoff, J. (1986). New empirical model for the structural properties of silicon. *Physical Review Letters*, 56, 632.
- Tersoff, J. (1988a). Empirical interatomic potential for silicon with improved elastic properties. *Physical Review B*, 38, 9902.
- Tersoff, J. (1988b). New empirical approach for the structure and energy of covalent systems. *Physical Review B*, 37, 6991.

- Tersoff, J. (1989). Modeling solid-state chemistry: Interatomic potential for multicomponent systems. *Physical Review B*, 39, 5566.
- Verlet, L. (1967). Computer 'experiments' on classical fluids. II equilibrium correlation functions. *Physical Review*, 159, 98.
- Xing, Y., & Rosner, D. E. (1999). Prediction of spherule size in gas phase nanoparticle synthesis. *Journal of Nanoparticle Research*, 2, 277.
- Xiong, Y., Akhtar, M. K., & Pratsinis, S. E. (1993). Formation of agglomerate particles by coagulation and sintering. Part II. The evolution of the morphology of aerosol-made titania, silica, and silica-doped titania powders. *Journal of Aerosol Science*, 24, 301.
- Yadha, V., & Helble, J. J. (2004). Modeling the coalescence of heterogeneous amorphous particles. *Journal of Aerosol Science*, 35, 665.
- Zachariah, M. R., & Carrier, M. J. (1999). Molecular dynamics computation of gas-phase nanoparticles sintering: A comparison with phenomenological models. *Journal of Aerosol Science*, 30, 1139.